

THE OH MEGAMASER LUMINOSITY FUNCTION

JEREMY DARLING & RICCARDO GIOVANELLI

Department of Astronomy and National Astronomy and Ionosphere Center, Cornell University, Ithaca, NY
 14853; darling@astro.cornell.edu; riccardo@astro.cornell.edu

Submitted to the Astrophysical Journal, 22 January 2002; accepted 21 February 2002.

ABSTRACT

We present the 1667 MHz OH megamaser luminosity function derived from a single flux-limited survey. The Arecibo Observatory OH megamaser (OHM) survey has doubled the number of known OH megamasers, and we list the complete catalog of OHMs detected by the survey here, including three redetections of known OHMs. OHMs are produced in major galaxy mergers which are (ultra)luminous in the far-infrared. The OH luminosity function follows a power law in integrated line luminosity, $\Phi \propto L_{OH}^{-0.64}$ Mpc⁻³ dex⁻¹, and is well-sampled for $10^{2.2} L_{\odot} < L_{OH} < 10^{3.8} L_{\odot}$. The OH luminosity function is incorporated into predictions of the detectability and areal density of OHMs in high redshift OH surveys for a variety of current and planned telescopes and merging evolution scenarios parameterized by $(1+z)^m$ in the merger rate ranging from $m = 0$ (no evolution) to $m = 8$ (extreme evolution). Up to dozens of OHMs may be detected per square degree per 50 MHz by a survey reaching an *rms* noise of 100 μ Jy per 0.1 MHz channel. An adequately sensitive “OH Deep Field” would significantly constrain the evolution exponent m even if no detections are made. In addition to serving as luminous tracers of massive mergers, OHMs may also trace highly obscured nuclear starburst activity and the formation of binary supermassive black holes.

Subject headings: masers — galaxies: interactions — galaxies: evolution — galaxies: luminosity function — galaxies: starburst — radio lines: galaxies

1. INTRODUCTION

OH megamasers are luminous masing lines at 1667 and 1665 MHz which are at least a million times more luminous than typical OH masers associated with compact HII regions. OH megamasers (OHMs) are produced in (ultra)luminous infrared galaxies ([U]LIRGs), major galaxy mergers undergoing extreme bursts of circumnuclear star formation. OH megamasers are especially promising as tracers of dust obscured star formation and merging galaxies because they can potentially be observed at high redshifts with modern radio telescopes in reasonable integration times, they *favor* regions of high dust opacity where ultraviolet, optical, and even near-IR emission can be extremely difficult to detect, and their detection automatically provides an accurate redshift measurement. The Arecibo Observatory¹ OH megamaser survey is a flux-limited survey designed to quantify the relationships between merging galaxies and the OH megamasers (OHMs) they produce with the goal of using OHMs as luminous tracers of mergers at high redshifts (Darling & Giovanelli 2000, 2001, 2002; hereafter Papers I, II, III). Central to the application of OHMs as tracers of merging galaxies at various redshifts is a measurement of the low redshift OH luminosity function.

The Arecibo OH megamaser survey is the first survey with adequate statistics to construct an OH luminosity function (LF) from a flux-limited sample. Baan (1991) computed a OH luminosity function from the 48 OHMs which were known at the time under the assumption that they constituted a flux-limited sample and that the fraction of LIRGs showing detectable OHMs is constant. Baan’s OH LF has a Schechter-type profile which is slowly falling from $L_{OH} = 10^0$ – $10^2 L_{\odot}$, has a knee at

roughly $10^{2.5} L_{\odot}$, and a steep falloff out to $10^4 L_{\odot}$. We are now in a position to recompute the OH LF from a single complete survey with well-defined selection criteria extracted from the PSCz, a flux-limited catalog which also has well-defined selection criteria (Saunders *et al.* 2000). An OH LF will be a useful guide for deep surveys for OHMs which can be related to the merging history of galaxies, the dust-obscured star formation history of the Universe, and the production of some portions of the low frequency gravitational wave background.

This paper presents an overview of the Arecibo OH megamaser survey, focusing on the issues pertinent to constructing an OH luminosity function (OH LF) from the survey results. Selection methods and the complete catalog of detected OHMs are presented in §2. Section 3 discusses the methods used to compute the OH luminosity function, presents the OH LF, and compares it to previous results for OHMs and ULIRGs. The OH LF is then applied to the problem of detecting OHMs at high redshift in §4 and some discussion is made of the utility of OHMs as tracers of galaxy evolution, including merging, dust-obscured nuclear starbursts, and the formation of binary supermassive black holes.

Note that Papers I–III assume a cosmology with $H_0 = 75$ km s⁻¹ Mpc⁻¹, $q_0 = 0$, and $\Omega_{\Lambda} = 0$ for ease of comparison with previous (U)LIRG surveys such as Kim & Sanders (1998). This analysis, however, assumes a more likely cosmology which is flat but accelerating: $\Omega_M = 0.3$ and $\Omega_{\Lambda} = 0.7$. All of the OHM data presented here have been converted to this cosmology.

2. THE ARECIBO OH MEGAMASER SURVEY

Papers I–III present a survey for OHMs conducted at the Arecibo Observatory covering one quarter of the sky to a depth of roughly one gigaparsec. The survey doubles the number of known OH megamasers and quantifies the

¹ The Arecibo Observatory is part of the National Astronomy and Ionosphere Center, which is operated by Cornell University under a cooperative agreement with the National Science Foundation.

relationship between luminous infrared galaxies and OH megamasers. The survey builds the foundation required to employ OH megamasers as tracers of major galaxy mergers, dust-obscured star formation, and the formation of binary supermassive black holes spanning the epoch of galaxy evolution to the present. Here we present details of the survey relevant to constructing an OH LF: the candidate selection criteria and the complete catalog of detected OHMs with properties converted to a flat $\Omega_\Lambda = 0.7$ cosmology.

2.1. Candidate Selection

For the Arecibo OH megamaser survey, candidates were selected from the Point Source Catalog redshift survey (PSCz; Saunders *et al.* 2000), supplemented by the NASA/IPAC Extragalactic Database.² The PSCz catalog is a flux-limited ($IRAS\ f_{60\mu m} > 0.6$ Jy) redshift survey of 15,000 *IRAS* galaxies over 84% of the sky (see Saunders *et al.* 2000). We select *IRAS* sources which are in the Arecibo sky ($0^\circ < \delta < 37^\circ$), were detected at 60 μm , and have $0.1 \leq z \leq 0.45$. The lower redshift bound is set to avoid local radio frequency interference (RFI), while the upper bound is set by the bandpass of the wide L-band receiver at Arecibo, although an effective upper bound is imposed around $z = 0.23$ by the radio frequency interference (RFI) environment, as discussed in §3.3. No constraints are placed on FIR colors or luminosity. The redshift requirement limits the number of candidates in the Arecibo sky to 311. The condition that candidates have $z > 0.1$ automatically selects (U)LIRGs if they are included in the PSCz. The strong influence of L_{FIR} on OHM fraction in LIRGs (see Paper III) is the primary reason for our high detection rate compared to previous surveys (e.g. Staveley-Smith *et al.* 1992; Baan, Haschick, & Henkel 1992).

2.2. OH Megamaser Detections

Tables 1 and 2 list respectively the optical/FIR and radio properties of the 50 new OHM detections and 3 re-detections. Note that OHM *IRAS* F11180+1623 is *not* in the PSCz sample, but was observed along with other OHM candidates not found in the PSCz sample to fill in telescope time when local sidereal time coverage of the official sample was sparse. This detection is not included in any of the survey statistics or interpretation, including the OH LF. Spectra of the 53 OHMs appear in Papers I, II, and III. Table 1 lists the optical redshifts and FIR properties of the non-detections in the following format: Column (1): *IRAS* Faint Source Catalog (FSC) name. Columns (2) and (3): Source coordinates (epoch B1950.0) from the FSC, or the Point Source Catalog (PSC) if unavailable in the FSC.

Columns (4), (5) and (6): Heliocentric optical redshift, reference, and corresponding velocity. Uncertainties in velocities are listed whenever they are available.

Column (7): Cosmic microwave background rest-frame velocity. This is computed from the heliocentric velocity using the solar motion with respect to the CMB measured

by Lineweaver *et al.* (1996): $cz_\odot = 368.7 \pm 2.5$ km s⁻¹ towards $(l, b) = (264^\circ 31' \pm 0^\circ 16', 48^\circ 05' \pm 0^\circ 09')$.

Column (8): Luminosity distance computed from z_{CMB} via

$$D_L = (1 + z_{CMB}) \frac{c}{H_0} \int_0^{z_{CMB}} [(1 + z')^3 \Omega_M + \Omega_\Lambda]^{-\frac{1}{2}} dz', \quad (1)$$

assuming $\Omega_M = 0.3$ and $\Omega_\Lambda = 0.7$.

Columns (9) and (10): *IRAS* 60 and 100 μm flux densities in Jy. FSC flux densities are listed whenever they are available. Otherwise, PSC flux densities are used. Uncertainties refer to the last digits of each measure, and upper limits on 100 μm flux densities are indicated by a “less-than” symbol.

Column (11): The logarithm of the far-infrared luminosity in units of $h_{75}^{-2} L_\odot$. L_{FIR} is computed following the prescription of Fullmer & Lonsdale (1989): $L_{FIR} = 3.96 \times 10^5 D_L^2 (2.58 f_{60} + f_{100})$, where f_{60} and f_{100} are the 60 and 100 μm flux densities expressed in Jy, D_L is in h_{75}^{-1} Mpc, and L_{FIR} is in units of $h_{75}^{-2} L_\odot$. If f_{100} is only available as an upper limit, the permitted range of L_{FIR} is listed. The lower bound on L_{FIR} is computed for $f_{100} = 0$ Jy, and the upper bound is computed with f_{100} set equal to its upper limit. The uncertainties in D_L and in the *IRAS* flux densities typically produce an uncertainty in $\log L_{FIR}$ of 0.03.

Table 2 lists the OH emission properties and 1.4 GHz flux density of the OH detections in the following format: Column (1): *IRAS* FSC name.

Column (2): Measured heliocentric velocity of the 1667.359 MHz line, defined by the center of the FWHM of the line. The uncertainty in the velocity of the line center is estimated assuming an uncertainty of ± 1 channel (± 49 kHz) on each side of the line. Although one can generally determine emission line centers with much higher precision when the shapes of lines are known, OHM line profiles are asymmetric, multi-component, and non-gaussian (see Papers I–III). They defy simple shape descriptions, so we use this conservative and basic prescription to quantify the uncertainty in the line centers.

Column (3): Peak flux density of the 1667 MHz OH line in mJy.

Column (4): Equivalent width-like measure in MHz. W_{1667} is the ratio of the integrated 1667 MHz line flux to its peak flux. Ranges are listed for W_{1667} in cases where the identification of the 1665 MHz line is unclear, but in many cases the entire emission structure is included in W_{1667} as indicated in the discussion of each source in Papers I–III.

Column (5): Observed FWHM of the 1667 MHz OH line in MHz.

Column (6): Rest frame FWHM of the 1667 MHz OH line in km s⁻¹. The rest frame width was calculated from the observed width as $\Delta v_{rest} = c(1 + z)(\Delta \nu_{obs}/\nu_o)$.

Column (7): Hyperfine ratio, defined by $R_H = F_{1667}/F_{1665}$, where F_ν is the integrated flux density across the emission line centered on ν . $R_H = 1.8$ in thermodynamic equilibrium. In many cases, the 1665 MHz OH line is not apparent, or is blended into the 1667 MHz OH line, and a good measure of R_H becomes difficult without a model for the line profile. It is also not clear that the two lines should have similar profiles, particularly if the lines are aggregates of many emission regions in different satura-

² The NASA/IPAC Extragalactic Database (NED) is operated by the Jet Propulsion Laboratory, California Institute of Technology, under contract with the National Aeronautics and Space Administration.

TABLE 1
ARECIBO SURVEY OH MEGAMASERS: OPTICAL REDSHIFTS AND FIR PROPERTIES

<i>IRAS</i> Name FSC (1)	α B1950 (2)	δ B1950 (3)	z_{\odot} (4)	Ref z (5)	$c z_{\odot}$ km/s (6)	$c z_{CMB}$ km/s (7)	D_L h_{75}^{-1} Mpc (8)	$f_{60\mu m}$ Jy (9)	$f_{100\mu m}$ Jy (10)	$\log L_{FIR}$ $h_{75}^{-2} L_{\odot}$ (11)
01562+2528	01 56 12.0	+25 27 59	0.1658	1	49707(505)	49441(506)	739(8)	0.809(57)	1.62(24)	11.90
02524+2046	02 52 26.8	+20 46 54	0.1815	1	54421(125)	54213(129)	788(2)	0.958(77)	< 4.79	11.81–12.28
03521+0028	03 52 08.5	+00 28 21	0.1522	2	45622(138)	45501(142)	674(2)	2.638(237)	3.83(34)	12.28
03566+1647	03 56 37.8	+16 47 57	0.1335	1	40033(54)	39911(65)	585(1)	0.730(66)	< 2.37	11.40–11.75
04121+0223	04 12 10.5	+02 23 12	0.1216	3	36454(250)	36362(253)	529(4)	0.889(62)	< 2.15	11.40–11.69
06487+2208	06 48 45.1	+22 08 06	0.1437	4	43080(300)	43206(302)	637(5)	2.070(166)	2.36(26)	12.10
07163+0817	07 16 23.7	+08 17 34	0.1107	1	33183(110)	33367(115)	482(2)	0.891(89)	1.37(11)	11.53
07572+0533	07 57 17.9	+05 33 16	0.1894	1	56783(122)	57022(126)	865(2)	0.955(76)	1.30(20)	12.04
08201+2801	08 20 10.1	+28 01 19	0.1680	5	50365(70)	50583(77)	757(1)	1.171(70)	1.43(16)	12.00
08279+0956	08 27 56.1	+09 56 41	0.2085	1	62521(107)	62788(110)	963(2)	0.586(64)	< 1.26	11.75–12.01
08449+2332	08 44 55.6	+23 32 12	0.1510	1	45277(102)	45530(106)	675(2)	0.867(69)	1.20(17)	11.79
08474+1813	08 47 28.3	+18 13 14	0.1450	5	43470(70)	43739(75)	646(1)	1.279(115)	1.54(18)	11.91
09039+0503	09 03 56.4	+05 03 28	0.1250	5	37474(70)	37781(73)	551(1)	1.484(89)	2.06(21)	11.86
09531+1430	09 53 08.3	+14 30 22	0.2151	1	64494(148)	64818(149)	998(2)	0.777(62)	1.04(14)	12.08
09539+0857	09 53 54.9	+08 57 23	0.1290	5	38673(70)	39008(72)	570(1)	1.438(101)	1.04(18)	11.79
10035+2740	10 03 36.7	+27 40 19	0.1662	1	49826(300)	50116(301)	750(5)	1.144(126)	1.63(161)	12.01
10339+1548	10 33 58.1	+15 48 11	0.1965	1	58906(122)	59242(123)	903(2)	0.977(59)	1.35(16)	12.09
10378+1108 ^a	10 37 49.1	+11 09 08	0.1362	2	40843(61)	41190(62)	605(1)	2.281(137)	1.82(18)	12.05
11028+3130	11 02 54.0	+31 30 40	0.1990	5	59659(70)	59948(73)	915(1)	1.021(72)	1.44(16)	12.13
11180+1623 ^b	11 18 06.7	+16 23 16	0.1660	5	49766(70)	50104(71)	749(1)	1.189(95)	1.60(18)	12.02
11524+1058	11 52 29.6	+10 58 22	0.1784	1	53479(134)	53823(135)	811(2)	0.821(66)	1.17(15)	11.93
12005+0009	12 00 30.2	+00 09 24	0.1226	1	36759(177)	37116(177)	540(3)	0.736(88)	0.98(15)	11.52
12018+1941 ^a	12 01 51.8	+19 41 46	0.1686	6	50559(65)	50880(67)	762(1)	1.761(123)	1.78(23)	12.16
12032+1707	12 03 14.9	+17 07 48	0.2170	5	65055(70)	65382(72)	1008(1)	1.358(95)	1.54(19)	12.31
12162+1047	12 16 13.9	+10 47 58	0.1465	1	43931(149)	44267(150)	654(2)	0.725(58)	< 0.95	11.50–11.68
12549+2403	12 54 53.4	+24 03 57	0.1317	1	39491(145)	39772(147)	582(2)	0.739(66)	1.03(13)	11.60
13218+0552	13 21 48.4	+05 52 40	0.2051	6	61488(58)	61788(62)	946(1)	1.174(82)	0.71(14)	12.13
14043+0624	14 04 20.0	+06 24 48	0.1135	1	34025(114)	34283(117)	496(2)	0.795(64)	1.31(16)	11.51
14059+2000	14 05 56.4	+20 00 42	0.1237	1	37084(89)	37316(93)	543(1)	0.857(120)	1.88(32)	11.68
14070+0525 ^a	14 07 00.3	+05 25 40	0.2655	1	79591(400)	79847(401)	1264(7)	1.447(87)	1.82(18)	12.55
14553+1245	14 55 19.1	+12 45 21	0.1249	1	37449(133)	37636(136)	549(2)	0.888(53)	1.17(16)	11.62
14586+1432	14 58 41.6	+14 31 53	0.1477	1	44287(118)	44467(122)	658(2)	0.569(91)	1.07(17)	11.64
15224+1033	15 22 27.4	+10 33 17	0.1348	1	40405(155)	40559(158)	595(2)	0.737(74)	0.72(15)	11.57
15587+1609	15 58 45.5	+16 09 23	0.1375	1	41235(195)	41329(198)	607(3)	0.740(52)	0.82(21)	11.60
16100+2527	16 10 00.4	+25 28 02	0.1310	3	39272(250)	39338(252)	575(4)	0.715(50)	< 1.38	11.39–11.63
16255+2801	16 25 34.0	+28 01 32	0.1340	1	40186(122)	40226(127)	590(2)	0.885(88)	1.26(26)	11.69
16300+1558	16 30 05.6	+15 58 02	0.2417	6	72467(64)	72515(73)	1133(1)	1.483(134)	1.99(32)	12.47
17161+2006	17 16 05.8	+20 06 04	0.1098	1	32928(113)	32903(118)	475(2)	0.632(44)	< 1.37	11.16–11.43
17539+2935	17 54 00.1	+29 35 50	0.1085	6	32525(58)	32441(67)	467(1)	1.162(58)	1.36(19)	11.58
18368+3549	18 36 49.5	+35 49 36	0.1162	2	34825(40)	34688(51)	502(1)	2.233(134)	3.83(27)	11.98
18588+3517	18 58 52.4	+35 17 04	0.1067	6	31973(35)	31810(46)	458(1)	1.474(103)	1.75(33)	11.66
20248+1734	20 24 52.3	+17 34 24	0.1208	6	36219(87)	35943(90)	522(1)	0.743(82)	2.53(38)	11.68
20286+1846	20 28 39.9	+18 46 37	0.1347	1	40396(127)	40117(129)	588(2)	0.925(74)	2.25(16)	11.81
20450+2140	20 45 00.1	+21 40 03	0.1284	1	38480(111)	38189(113)	557(2)	0.725(51)	1.90(15)	11.67
21077+3358	21 07 45.9	+33 58 05	0.1764	1	52874(117)	52587(119)	791(2)	0.885(88)	< 1.55	11.75–11.98
21272+2514	21 27 15.1	+25 14 39	0.1508	1	45208(120)	44890(121)	664(2)	1.075(118)	< 1.63	11.69–11.89
22055+3024	22 05 33.6	+30 24 52	0.1269	1	38041(24)	37715(29)	550(0)	1.874(356)	2.32(23)	11.93
22116+0437	22 11 38.6	+04 37 29	0.1939	1	58144(118)	57787(118)	878(2)	0.916(73)	< 1.03	11.85–12.01
23019+3405	23 01 57.3	+34 05 27	0.1080	6	32389(28)	32061(32)	462(0)	1.417(99)	2.11(38)	11.69
23028+0725	23 02 49.2	+07 25 35	0.1496	1	44845(198)	44476(198)	658(3)	0.914(100)	< 1.37	11.61–11.81
23129+2548	23 12 54.4	+25 48 13	0.1790	5	53663(70)	53314(71)	803(1)	1.811(145)	1.64(44)	12.21
23199+0123	23 19 57.7	+01 22 57	0.1367	3	40981(250)	40614(250)	596(4)	0.627(63)	1.03(16)	11.58
23234+0946	23 23 23.6	+09 46 15	0.1279	6	38356(24)	37988(24)	554(0)	1.561(94)	2.11(30)	11.88

^aA known OHM included in the survey sample.

^b*IRAS* 11180+1623 is not in the PSCz catalog (excluded by the PSCz mask; Saunders *et al.* 2000). It is in the 1 Jy survey (Kim & Sanders 1998).

REFERENCES.—Redshifts were obtained from: (1) Saunders *et al.* 2000; (2) Strauss *et al.* 1992; (3) Lawrence *et al.* 1999; (4) Lu & Freudling 1995; (5) Kim & Sanders 1998; (6) Fisher *et al.* 1995.

TABLE 2
ARECIBO SURVEY OH MEGAMASERS: OH LINE AND 1.4 GHz CONTINUUM PROPERTIES

<i>IRAS</i> Name FSC (1)	$cz_{1667, \odot}$ km/s (2)	f_{1667} mJy (3)	W_{1667} MHz (4)	$\Delta\nu_{1667}^a$ MHz (5)	Δv_{1667}^b km/s (6)	R_H (7)	$\log L_{FIR}$ $h_{75}^{-2} L_{\odot}$ (8)	$\log L_{OH}$ $h_{75}^{-2} L_{\odot}$ (9)	$f_{1.4GHz}^c$ mJy (10)
01562+2528	49814(15)	6.95	1.29	1.04	218	5.9	11.90	3.25	6.3(0.5)
02524+2046	54162(15)	39.82	0.50	0.36	76	3.2	11.81–12.28	3.74	2.9(0.6)
03521+0028	45512(14)	2.77	0.61	0.29	59	5.8	12.28	2.44	6.7(0.6)
03566+1647	39865(14)	1.96	0.98	0.23	48	\gtrsim 9.6	11.40–11.75	2.32	3.5(0.5)
04121+0223	36590(14)	2.52	0.76	1.04	209	2.9	11.40–11.69	2.32	3.1(0.5)
06487+2208	42972(14)	6.98	0.66	0.37	76	8.0	12.10	2.82	10.8(0.6)
07163+0817	33150(14)	4.00	0.69	0.12	24	\sim 5.5	11.53	2.37	3.5(0.5)
07572+0533	56845(15)	2.26	1.03	0.73	156	\gtrsim 10.4	12.04	2.74	< 5.0
08201+2801	50325(15)	14.67	0.97–1.19	0.98	205	\gtrsim 8.2	12.00	3.45	16.7(0.7)
08279+0956	62422(15)	4.79	1.02	0.95	207	5.9	11.75–12.01	3.23	4.4(0.8)
08449+2332	45424(14)	2.49	1.09	0.47	97	\gtrsim 11.0	11.79	2.59	6.1(0.5)
08474+1813	43750(14)	2.20	1.29–1.70	1.98	409	\gtrsim 3.0	11.91	2.70	4.2(0.5)
09039+0503	37720(14)	5.17	1.23	1.05	212	8.5	11.86	2.83	6.6(0.5)
09531+1430	64434(15)	3.98	1.03	1.17	256	\sim 3.4	12.08	3.42	3.0(0.5)
09539+0857	38455(14)	14.32	1.47	1.56	317	2.5	11.79	3.48	9.5(1.2)
10035+2740	50065(14)	2.29	0.74	0.31	65	\gtrsim 15.4	12.01	2.50	6.3(0.5)
10339+1548	58983(15)	6.26	0.28	0.19	40	\gtrsim 14.5	12.09	2.65	5.1(0.5)
10378+1108 ^d	40811(14)	19.70	1.50	0.87	177	\dots	12.05	3.54	8.9(0.6)
11028+3130	59619(15)	4.27	0.72	0.41	89	5.5	12.13	2.97	< 5.0
11180+1623 ^e	49783(14)	1.82	0.42	0.61	127	\gtrsim 5.1	12.02	2.34	4.2(0.5)
11524+1058	53404(15)	3.17	1.21	1.32	279	\gtrsim 4.9	11.93	2.98	< 5.0
12005+0009	36472(14)	3.51	0.71	0.41	82	\sim 2.0	11.52	2.62	5.4(0.6)
12018+1941 ^d	50317(15)	2.63	0.81	0.86	181	\gtrsim 5.6	12.16	2.59	6.5(0.5)
12032+1707	64920(15)	16.27	2.69	3.90	853	\dots	12.31	4.15	28.7(1.0)
12162+1047	43757(14)	2.07	0.64	0.51	105	\gtrsim 11.1	11.50–11.68	2.25	6.8(1.6)
12549+2403	39603(14)	1.79	0.89	0.50	102	\sim 2.6	11.60	2.37	3.7(0.5)
13218+0552	61268(15)	4.01	2.49	1.45	314	\dots	12.13	3.45	5.3(0.5)
14043+0624	33912(14)	2.75	0.33	0.27	54	1.4	11.51	2.10	15.6(1.0)
14059+2000	37246(14)	15.20	1.10	0.80	161	5.3	11.68	3.34	7.5(0.5)
14070+0525 ^d	79929(16)	8.37	3.21	2.62	596	\dots	12.55	4.13	4.0(0.6)
14553+1245	37462(14)	2.93	0.39	0.38	77	\gtrsim 14.5	11.62	2.27	3.8(0.5)
14586+1432	44380(14)	7.11	< 2.67	1.79	369	\dots	11.64	3.41	11.1(0.6)
15224+1033	40290(14)	12.27	0.73–0.80	0.15	31	\gtrsim 9.5	11.57	3.04	3.6(0.5)
15587+1609	40938(14)	13.91	0.99	0.86	176	6.9	11.60	3.26	< 5.0
16100+2527	40040(14)	2.37	0.60	0.23	46	3.2	11.39–11.63	2.29	< 5.0
16255+2801	40076(14)	7.02	0.45	0.39	79	\gtrsim 13.7	11.69	2.57	< 5.0
16300+1558	72528(15)	3.12	0.56	0.59	131	\dots	12.47	2.85	7.9(0.5)
17161+2006	32762(14)	4.84	0.62	0.38	76	\sim 6.2	11.16–11.43	2.39	7.3(0.6)
17539+2935	32522(14)	0.76	0.72	0.81	161	\gtrsim 2.9	11.58	1.76	4.0(0.6)
18368+3549	34832(14)	4.58	1.79	2.10	421	\gtrsim 9.5	11.98	2.85	21.0(0.8)
18588+3517	31686(14)	7.37	0.56	0.32	64	5.1	11.66	2.52	5.9(0.5)
20248+1734	36538(14)	2.61	1.36	0.88	177	\sim 6.8	11.68	2.53	< 5.0
20286+1846	40471(14)	15.58	1.51	1.10	224	\gtrsim 4.4	11.81	3.41	< 5.0
20450+2140	38398(14)	2.27	0.67	0.71	144	6.2	11.67	2.24	5.0(0.5)
21077+3358	52987(15)	5.04	1.86	1.15	243	7.4	11.75–11.98	3.26	9.4(1.0)
21272+2514	45032(14)	16.33	1.87	1.27	263	13.7	11.69–11.89	3.66	4.4(0.5)
22055+3024	37965(14)	6.35	0.77	0.46	92	6.2	11.93	2.73	6.4(0.5)
22116+0437	58180(15)	1.76	1.16	0.56	121	\sim 5.2	11.85–12.01	2.77	8.4(0.6)
23019+3405	32294(14)	3.58	0.52	0.28	57	\gtrsim 15.6	11.69	2.12	7.7(0.5)
23028+0725	44529(14)	8.69	1.09	1.06	219	1.9	11.61–11.81	3.29	19.5(1.1)
23129+2548	53394(15)	4.59	2.0	1.78	376	\dots	12.21	3.27	4.7(0.5)
23199+0123	40680(14)	1.80	0.82	0.68	139	\sim 2.3	11.58	2.38	3.0(0.5)
23234+0946	38240(14)	3.32	1.23	1.32	266	2.4	11.88	2.75	11.6(1.0)

^aThe frequency width $\Delta\nu_{1667}$ is the *observed* FWHM.

^bThe velocity width Δv_{1667} is the *rest frame* FWHM. The rest frame and observed widths are related by $\Delta v_{rest} = c(1+z)(\Delta\nu_{obs}/\nu_o)$.

^c1.4 GHz continuum fluxes are courtesy of the NRAO VLA Sky Survey (Condon *et al.* 1998).

^dRedetection of a known OHM included in the survey sample.

^e*IRAS* 11180+1623 is not in the PSCz catalog (excluded by the PSCz mask; Saunders *et al.* 2000). It is in the 1 Jy survey (Kim & Sanders 1998).

tion states. Some spectra allow a lower limit to be placed on R_H , indicated by a “greater than” symbol. Blended or noisy lines have uncertain values of R_H , and are indicated by a tilde, but in some cases, separation of the two OH lines is impossible and no value is listed for R_H .

Column (8): Logarithm of the FIR luminosity, as in Table 1.

Column (9): Logarithm of the measured isotropic OH line luminosity, which includes the integrated flux density of both the 1667.359 and the 1665.4018 MHz lines.

Column (10): 1.4 GHz continuum fluxes from the NRAO VLA Sky Survey (Condon *et al.* 1998). If no continuum source lies within $30''$ of the *IRAS* coordinates, an upper limit of 5.0 mJy is listed.

3. THE OH LUMINOSITY FUNCTION

3.1. Computing a Spectral Line Luminosity Function

The luminosity function $\Phi(L)$ is the number density of objects with luminosity L per (logarithmic) interval in L . An unbiased direct measurement of $\Phi(L)$ would require that all objects with a given luminosity be detected within the survey volume, which is generally not possible in a flux-limited survey. Instead, each object in a survey has an effective volume in which it could have been detected by the survey, and the sum of detections weighted by their available volumes V_a determines the luminosity function. The most general unbiased maximum likelihood computation of a luminosity function is computed from V_a following the prescription (Page & Carrera 2000):

$$\Phi(L) = \frac{1}{\Delta \log L} \sum \frac{1}{V_a(L)} \quad (2)$$

where the sum is over the detected objects in the luminosity bin $\Delta \log L$ centered on L and redshift bin Δz centered on z . The uncertainty in the luminosity function is

$$\sigma_\Phi = \frac{1}{\Delta \log L} \left(\sum \frac{1}{V_a^2} \right)^{\frac{1}{2}}. \quad (3)$$

Computation of the volume available to each detection depends on the areal coverage of the survey Ω and the maximum detectable distance of each object detected ($D_{L,max}$ or z_{max}). The relationship between physical comoving volume and luminosity distance is given by

$$V = \frac{\Omega}{3} \left(\frac{D_L}{1+z} \right)^3 \quad (4)$$

only when $\Omega_k = 0$, where $\Omega_k = 1 - \Omega_M - \Omega_\Lambda$ (Weinberg 1972). From the definition of luminosity distance,

$$D_L \equiv \left(\frac{L}{4\pi S} \right)^{\frac{1}{2}} \quad (5)$$

for $\Omega_k = 0$, where L is the integrated line luminosity and S is the integrated line flux. Detection of spectral lines depends on the peak line flux density rather than the integrated line flux. The luminosity distance of Equation 5 must be modified by a factor $1+z$ in order to change to rest-frame luminosity density and flux density:

$$D_L = \left(\frac{L_{\nu_o}}{4\pi S_\nu} \right)^{\frac{1}{2}} (1+z)^{\frac{1}{2}}. \quad (6)$$

For a survey with sensitivity limit $n\sigma_\nu$, where σ_ν is the RMS noise flux density at frequency ν , and assuming that

this noise is independent of frequency, L_{ν_o} is an invariant quantity which relates the observed luminosity distance and peak flux density S_ν to the maximum detectable distance and the sensitivity limit $n\sigma_\nu$. We thus obtain an expression for the maximum detectable distance, $D_{L,max}$, which depends on itself through z_{max}

$$D_{L,max} = D_L \left(\frac{S_\nu}{n\sigma_\nu} \right)^{\frac{1}{2}} \left(\frac{1+z_{max}}{1+z} \right)^{\frac{1}{2}} \quad (7)$$

and must be solved such that $D_{L,max}$ can be related to observed quantities only. Equation 1 has no simple analytic solution for $\Omega_\Lambda \neq 0$ and must be solved numerically. Inserting this solution into Equation 7, we obtain a relation in z_{max} :

$$\begin{aligned} & \int_0^{z_{max}} [(1+z')^3 \Omega_M + \Omega_\Lambda]^{-\frac{1}{2}} dz' \\ &= \frac{H_0 D_L}{c\sqrt{1+z}} \left(\frac{S_\nu}{n\sigma_\nu} \right)^{\frac{1}{2}} (1+z_{max})^{-\frac{1}{2}} \end{aligned} \quad (8)$$

which has no analytical solution. The numerical solution for z_{max} (and the equivalent $D_{L,max}$) can be inserted into an expression for V_{max} obtained from Equation 4. Finally, we obtain the volume available to a given emission line source in the survey in the case where there is a minimum survey redshift z_{min} :

$$\begin{aligned} V_a &= V_{max} - V_{min} \\ &= \frac{\Omega}{3} \left[\left(\frac{D_{L,max}}{1+z_{max}} \right)^3 - \left(\frac{D_{L,min}}{1+z_{min}} \right)^3 \right]. \end{aligned} \quad (9)$$

Note that if z_{max} is greater than the upper bound in redshift of the survey, then we set z_{max} equal to this upper bound.

3.2. Computing a Continuum Luminosity Function

The procedure for computing a continuum luminosity function closely follows the steps for the emission line computation. The detection threshold is determined in the same manner, from a flux density sensitivity rather than an integrated flux. Unlike spectral line surveys, however, continuum surveys do not usually tune the bandpass to the redshift of each observed object. This introduces an error in computing the invariant luminosity from the measured flux because a different portion of the rest-frame spectral energy distribution is sampled for each object due to the redshift. A k-correction must be applied to the measured flux density to obtain the correct luminosity and hence to compute the maximum detectable distance for each source. The net k-correction between z and z_{max} will modify Equation 7 slightly

$$D_{L,max} = D_L \left(\frac{S_\nu \kappa}{n\sigma_\nu} \right)^{\frac{1}{2}} \left(\frac{1+z_{max}}{1+z} \right)^{\frac{1}{2}}, \quad (10)$$

but will add another wrinkle to the derivation of V_{max} in §3.1 because the k-correction will itself depend on D_L . We will approximate the k-correction to be constant at first, determine $D_{L,max}$, recompute the k-correction, and then correct $D_{L,max}$ if necessary. The k-correction is a weak function of $D_L - D_{L,max}$, and this single iteration approach to computing $D_{L,max}$ is adequate.

3.3. The OH Megamaser Luminosity Function

The Arecibo OH megamaser survey is a flux-limited survey for OH emission lines, but has three additional constraints: (1) objects observed in the survey are selected from a flux-limited 60 micron catalog (the PSCz; Saunders *et al.* 2000), (2) the survey has low and high redshift cutoffs at $z = 0.1$ and $z = 0.23$, and (3) the survey cannot include objects close to $z = 0.174$ where the OH lines are redshifted into the strong Galactic HI emission. The redshift cutoffs are imposed by radio frequency interference (RFI) encountered at Arecibo above 1510 MHz and below 1355 MHz. The typical RMS flux density for a 12 minute integration is 0.65 mJy, and detections are generally made at the 3σ level or greater, which is 2 mJy. These constraints are well-illustrated by Figure 1, which shows redshift cutoffs, the observable candidates, and the sensitivity limits in both OH line luminosity and FIR flux.

Ignoring constraint (1) for now, computation of the OH LF can follow the prescription outlined in §3.1 by setting the redshift bin Δz to span $z = 0.1$ to $z = 0.23$ with $z_{min} = 0.1$. We use $n\sigma_\nu = 2.0$ mJy and can effectively ignore the thin shell of space centered on $z = 0.174$ since its contribution to the total volume is negligible. The survey solid angle spans $0^\circ < \delta < 37^\circ$ such that $\Omega = 3.78$ steradians (30% of the sky).

Now fold in the PSCz selection criteria. First, the PSCz does not completely cover the $0^\circ < \delta < 37^\circ$ band. It excludes the galactic plane and areas with inadequate or

confused *IRAS* coverage (Saunders *et al.* 2000). The PSCz mask excludes 18% of the Arecibo coverage, reducing the survey solid angle to $\Omega = 3.21$ steradians (25.5% of the sky). The survey volume from $z = 0.1$ to $z = 0.23$ is thus 0.63 Gpc^3 .

Second, the PSCz has a $60 \mu\text{m}$ flux density limit of 0.6 Jy. Hence, the volume available to each object in the survey can potentially be limited by this cutoff rather than the OH line detectability. The true volume available to a given object in the survey is now

$$V_a = \min\{V_a^{OH}, V_a^{60\mu\text{m}}\}. \quad (11)$$

Computation of $V_a^{60\mu\text{m}}$ follows the continuum prescription outlined in §3.2, and the calculation of the LF uses this more restrictive definition of V_a . The luminosity bins $\Delta \log L$ refer to the integrated OH line luminosities of the OHMs. Hence, the details of detecting OHMs from both surveys are folded into V_a , and the luminosity intervals in the LF incorporate the information about the OH line luminosities.

Third, the *IRAS* $60 \mu\text{m}$ flux measurements require net k-corrections from D_L to $D_{L,max}$. The k-corrections themselves are derived from spectral energy distribution models for star forming galaxies developed by Dale *et al.* (2001). The models depend on the rest-frame FIR color $\log(f_{60\mu\text{m}}/f_{100\mu\text{m}})$ which is corrected from the observed color to the rest frame color using values tabulated by D. Dale (2001, private communication). The typical color correction from $z = 0.15$ to $z = 0$ for the OHM host sample is 0.05–0.10 (colors get “warmer”). The net k-correction for an OHM detected at $z = 0.15$ which is detectable to $z = 0.20$ with rest frame FIR color of -0.10 is $\kappa = 0.98$. Although the OHM sample spans a wide range of FIR colors, the net k-corrections vary little from source to source in the range $z = 0.1$ – 0.23 . Objects with no $100 \mu\text{m}$ detection generally have a range of possible net k-corrections centered on unity, which is adopted for lack of better information.

Figure 2 shows the OH luminosity, FIR luminosity, and redshift distributions of the OHM sample. Also shown are the maximum detectable redshift distributions computed from the OH detections, the $60 \mu\text{m}$ detections, and the available redshift distribution z_a . Note that the z_a distribution is quite flat but that the maximum detectable redshift distribution for OH indicates two populations of OHMs: a population which is just detected by the survey and indicates a large population of OHMs which would be detected by a deeper survey, and a population of “over-luminous” OHMs which can be detected in short integration times out to $z \simeq 1$, similar to QSOs or radio galaxies. Nearly half of the OHM sample falls into this interesting latter category. These are the objects which are useful for studies of galaxy evolution out to large redshifts. There is a hint of this population dichotomy in the plots of L_{OH} versus L_{FIR} analyzed in Paper III.

We combine all of the survey constraints and compute an OH LF which is presented in Figure 3. A power-law fit to the well-sampled OH LF points gives

$$\Phi = (9.8_{-7.5}^{+31.9} \times 10^{-6}) L_{OH}^{-0.64 \pm 0.21} \text{ Mpc}^{-3} \text{ dex}^{-1} \quad (12)$$

where L_{OH} is expressed in solar luminosities. The uniformity of the sampling in space is checked with the $\langle V/V_a \rangle$ test (Schmidt 1968). A uniformly distributed sample between 0 and 1 has mean 0.5. Hence, the $\langle V/V_a \rangle$ values

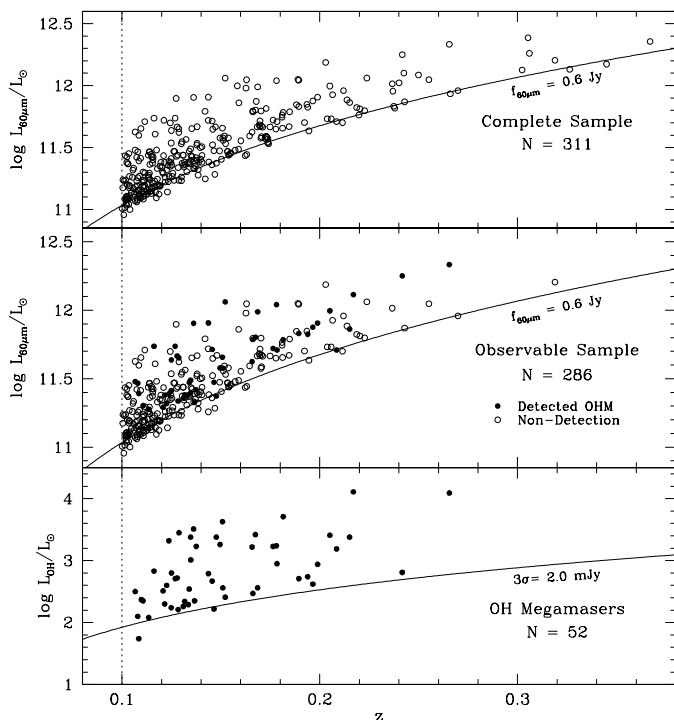


FIG. 1.— The Arecibo OH megamaser survey sample, observable candidates, and detected OH Megamasers. Shown are the $60 \mu\text{m}$ luminosities and the redshifts of the complete sample of OHM candidates extracted from the PSCz (*top*), the observable subset of these candidates which have unambiguous OH line properties (*middle*), and the OH line luminosities of the detected OHMs versus redshift (*bottom*). The dotted vertical lines indicate the $z = 0.1$ cutoff, and the solid lines indicate the flux density limits of the PSCz and the OHM survey.

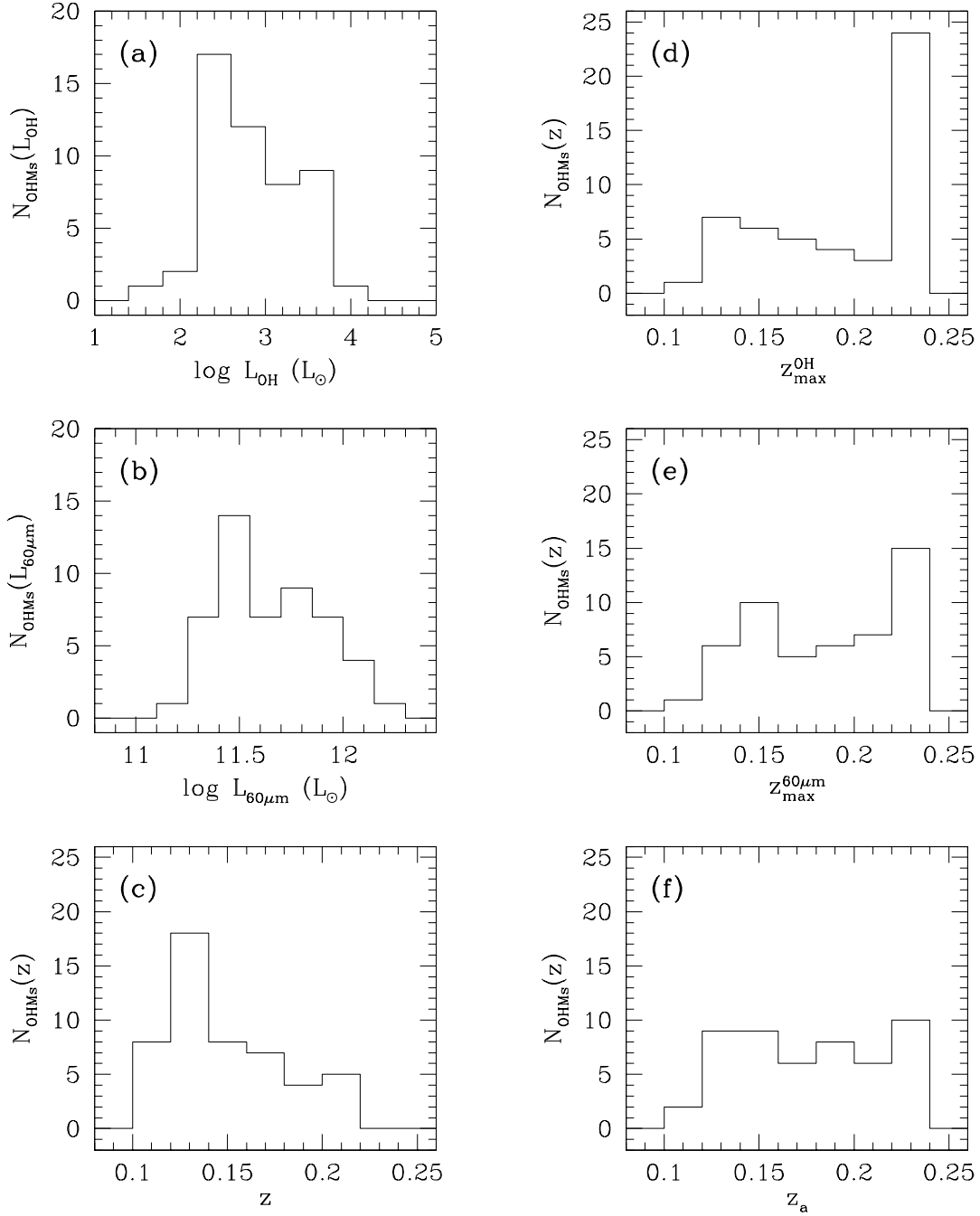


FIG. 2.— The OH megamaser sample: L_{OH} , $L_{60\mu\text{m}}$, redshift, and maximum detectable redshift distributions. Panels show: (a) The L_{OH} distribution of the survey OHM detections; (b) The $L_{60\mu\text{m}}$ distribution; (c) The redshift distribution; (d) The maximum detectable redshift distribution calculated from the OH emission line; (e) The maximum detectable redshift distribution calculated from the $60\mu\text{m}$ flux density; and (f) The available redshift distribution computed from $\min\{z_{\text{max}}^{\text{OH}}, z_{\text{max}}^{60\mu\text{m}}\}$. These distributions exclude two OHMs at $z > 0.23$.

consistent with 0.5 in well-sampled L_{OH} bins shown in Figure 3 indicate a uniformly distributed sample of OH megamasers. Both the OH LF and $\langle V/V_a \rangle$ are tabulated in Table 3, which includes the number of OHMs available in each L_{OH} bin.

OH LFs previously computed by Baan (1991) and Briggs (1998) show similar properties to the Arecibo OHM survey LF, as indicated in Figure 3. Baan’s OH LF samples a larger range of L_{OH} , showing a knee at roughly $10^{2.5}L_{\odot}$. The number of OHMs in the Arecibo sample contributing to the OH LF below $L_{\text{OH}} = 10^{2.2}L_{\odot}$ is in-

adequate to confirm this turnover in the LF. The survey sensitivity cutoff at these low line luminosities is severe, as seen in Figures 1 and 3. Also noteworthy is the higher OHM density found in the Arecibo LF versus Baan’s 1991 result for $L_{\text{OH}} > 10^3L_{\odot}$. Briggs (1998) derived an OH LF from a quadratic OH-FIR relation combined with a $60\mu\text{m}$ luminosity function derived by Koranyi & Strauss (1997). Briggs computes the OH LF analytically assuming an OHM fraction of unity in LIRGs for all $L_{60\mu\text{m}}$ (Figure 3b, *dotted line*) and numerically for an increasing OHM fraction versus $L_{60\mu\text{m}}$ (Figure 3b, *histogram*). Although a

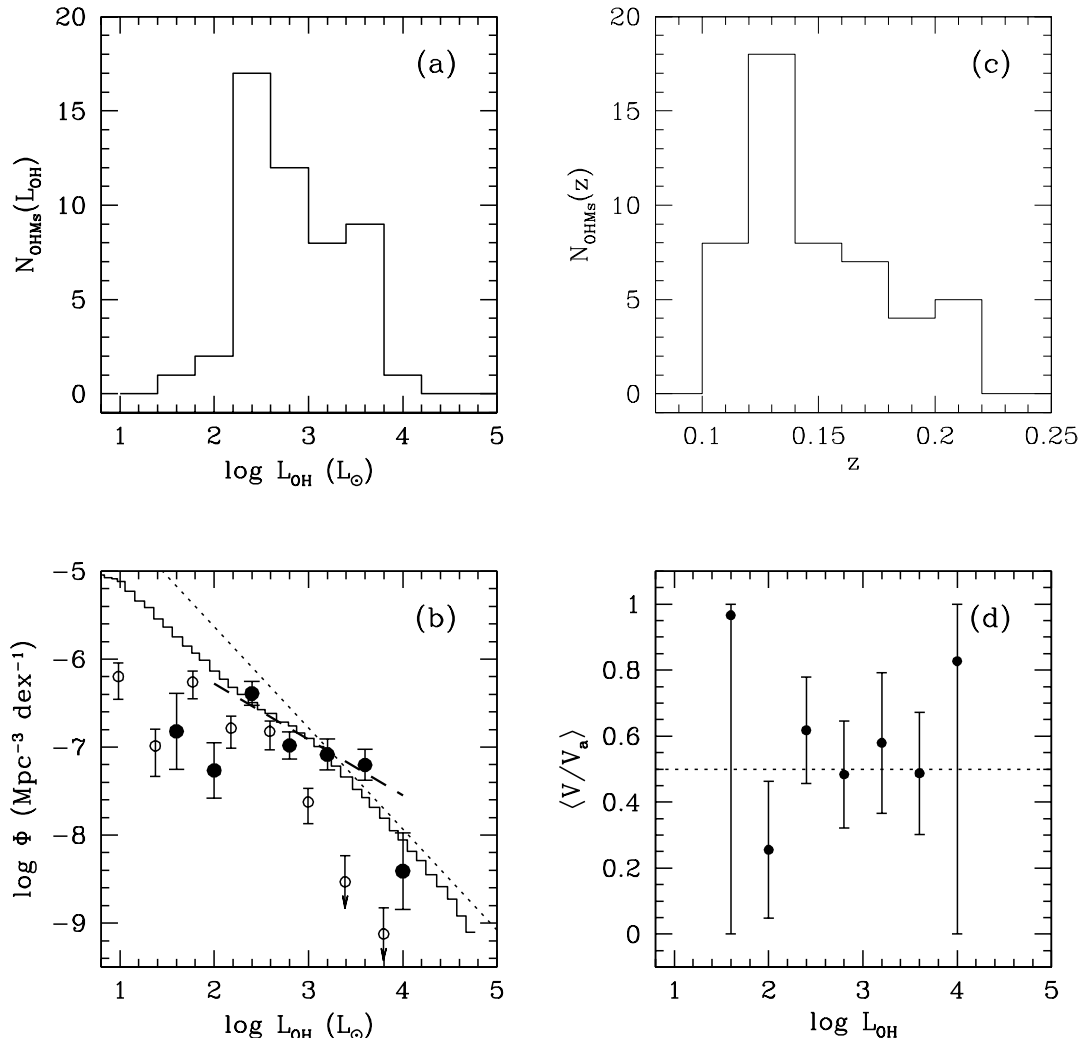


FIG. 3.— The OH megamaser luminosity function. Panels show: (a) The L_{OH} distribution of the survey OHM detections; (b) The OH luminosity function (*filled circles*) and a power-law fit to the well-sampled data points ($\Phi \propto L_{OH}^{-0.64}$; *dashed line*), the OH LF derived by Baan (1991; *open circles*), and the OH LF computed by Briggs (1998) for a fixed and variable OHM fraction in LIRGs (*dotted line and histogram, respectively*); (c) The redshift distribution; and (d) The average ratio of V to V_a which is consistent with 0.5 in well-sampled bins (a uniformly distributed sample has $\langle V/V_a \rangle = 0.5$). These distributions and calculations exclude two OHMs at $z > 0.23$.

quadratic OH-FIR relation is not supported by the known OHMs (Paper III), Briggs' OH LF follows the Arecibo OH LF data points remarkably closely above $L_{OH} = 10^2 L_{\odot}$. Briggs obtains a rough power-law slope of -1.15 , which is inconsistent with the Arecibo result of -0.64 ± 0.2 (Equation 12). The inconsistency can be attributed to the steep slope at the high luminosity end of the $60\mu\text{m}$ LF of Koranyi & Strauss (1997) compared to the shallower slope obtained by Yun, Reddy, & Condon (2001) and Kim & Sanders (1998). When translated into an OH LF, the steep $60\mu\text{m}$ slope is significantly lessened by Briggs's use of a quadratic OH-FIR relation. The Arecibo power-law slope for OHMs is consistent with the power-law LF Kim & Sanders (1998) determined for ULIRGs. They found $\Phi \propto L_{IR}^{-2.35 \pm 0.3} \text{ Mpc}^{-3} \text{ mag}^{-1}$ over $L_{IR} = 10^{12} - 10^{13} L_{\odot}$ (the exponent becomes -0.94 ± 0.12 when Φ is expressed in $\text{Mpc}^{-3} \text{ dex}^{-1}$).

A well-determined OH luminosity function forms the foundation of any galaxy evolution study which uses OH megamasers as luminous radio tracers of mergers, dust-enshrouded star formation, or supermassive black hole bi-

naries. We now use this new OH LF to predict the detectability and abundance of OHMs available to deep radio surveys.

4. DETECTING OH MEGAMASERS AT HIGH REDSHIFT

OH megamasers are excellent luminous tracers of merging galaxies. They may become a tool for measuring the merging history of galaxies across much of cosmic time and determine the contribution of merging supermassive black holes to the low frequency gravitational wave background and to low frequency gravitational wave bursts. They also provide an extinction-free tracer of bursts of highly obscured star formation and may provide an independent measure of the star formation history of the universe. Application of OH megamasers to these topics requires (1) that they be detectable at moderate to high redshifts, and (2) that their sky surface density be high enough for radio telescopes to detect at least a few per pointing.

4.1. Detectability with Current and Planned Facilities

TABLE 3
THE OH LUMINOSITY FUNCTION

$\log L_{OH}$ $h_{75}^{-2} L_{\odot}$	N(OHMs)	Φ $\text{Mpc}^{-3} \text{ dex}^{-1}$	$\langle V/V_a \rangle$
1.6	1	$(1.5 \pm 1.5) \times 10^{-7}$	$0.97 \pm \dots$
2.0	2	$(5.4 \pm 3.9) \times 10^{-8}$	0.26 ± 0.21
2.4	17	$(4.1 \pm 1.3) \times 10^{-7}$	0.62 ± 0.16
2.8	12	$(1.0 \pm 0.4) \times 10^{-7}$	0.48 ± 0.16
3.2	8	$(8.2 \pm 3.3) \times 10^{-8}$	0.58 ± 0.21
3.6	9	$(6.3 \pm 2.5) \times 10^{-8}$	0.49 ± 0.19
4.0	1	$(3.9 \pm 3.9) \times 10^{-9}$	$0.83 \pm \dots$

The detectability any given OH megamaser at high redshift depends on the strength of the OHM, the sensitivity of the instrumentation, and cosmology. Moving beyond $z \simeq 0.2$ requires a careful treatment of cosmology because the differences between luminosity distances and volumes among the manifold of possible cosmologies become significant. We assume for this analysis that $H_0 = 75 \text{ km s}^{-1} \text{ Mpc}^{-1}$, $\Omega_M = 0.3$, and $\Omega_\Lambda = 0.7$.

Assumptions are also required to translate the observed quantity, flux density, to a line luminosity. We assume that the integrated flux density can be approximated by the product of the peak flux density and an average rest-frame width, narrowed by the redshift:

$$F_{OH} = f_{OH} \frac{\Delta\nu_o}{1+z} = f_{OH} \frac{\nu_o \Delta\nu_o}{c(1+z)} \quad (13)$$

where the assumed rest-frame width is $\Delta\nu_o = 150 \text{ km s}^{-1}$.

Figure 4 plots sensitivity thresholds for a 3σ detection of an OHM with luminosity L_{OH} at redshift z . Included are the Arecibo OHM survey detections and sensitivity

limit, predictions for a 16 hour integration by the Giant Metrewave Radio Telescope (GMRT) at 610 and 327 MHz, predictions for a 12 minute integration by the Square Kilometer Array (SKA) down to 300 MHz, and predictions for a 16 hour integration by the Low Frequency Array (LOFAR) below 300 MHz. The GMRT is assumed to span 32 MHz with 0.12 MHz channels and obtain 0.083 mJy RMS noise per beam ($T_{sys} \simeq 100 \text{ K}$; Gain = 0.32 K Jy^{-1}).³ The SKA sensitivity is computed by scaling up the Arecibo OHM survey by a factor of 25 in collecting area but keeping all other parameters the same. Such a survey would have an RMS noise level of 0.027 mJy in 12 minutes of integration per 49 kHz channel. The sensitivity of LOFAR below 300 MHz is estimated from guidelines provided by M. P. van Haarlem⁴ to be 0.047 mJy RMS per 0.125 MHz channel in 16 hours of integration.

Note that, RFI environment and available receivers aside, Arecibo could detect OH gigamasers out to roughly $z = 1$ in a 12 minute integration. The GMRT shows much promise for the detection of $L_{OH} > 10^{3.5} L_{\odot}$ OHMs at $z = 1.7$ in an integration of 16 hours. In integration times of less than an hour, a SKA would be able to detect a large fraction of the OHM population out to medium redshifts and all OH gigamasers down to its lowest proposed operating frequency near 300 MHz. LOFAR would be able to detect OH gigamasers in roughly 32 hours of integration from $z \simeq 4.5$ back to the reionization epoch if they exist. Clearly OH megamasers are detectable at moderate redshifts with current facilities and at high redshifts with future arrays, but how abundant might they be?

4.2. The Sky Density of OH Megamasers

The OH megamaser luminosity function (OH LF) derived in §3 can predict the sky density of detectable OHMs as a function of instrument sensitivity, bandpass, and redshift. A useful function in terms of observational parameters would be the number of OHMs detected per square degree on the sky per MHz bandpass searched. This can be expressed as an integral of the OH LF over the range of detectable L_{OH} :

$$\begin{aligned} \frac{dN}{d\Omega d\nu} &= \int_{\log L_{OH,min}(z)}^{\log L_{OH,max}} \frac{dN}{d\Omega d\nu d\log L_{OH}} d\log L_{OH} \\ &= \int_{\dots}^{\dots} \frac{dN}{dV d\log L_{OH}} \frac{dV}{d\Omega d\nu} d\log L_{OH} \end{aligned}$$

³ See http://www.ncra.tifr.res.in/ncra_hp/ncra_hp/gmrt/gmrt_spec.html.

⁴ See <http://www.lofar.org/science/index.html>.

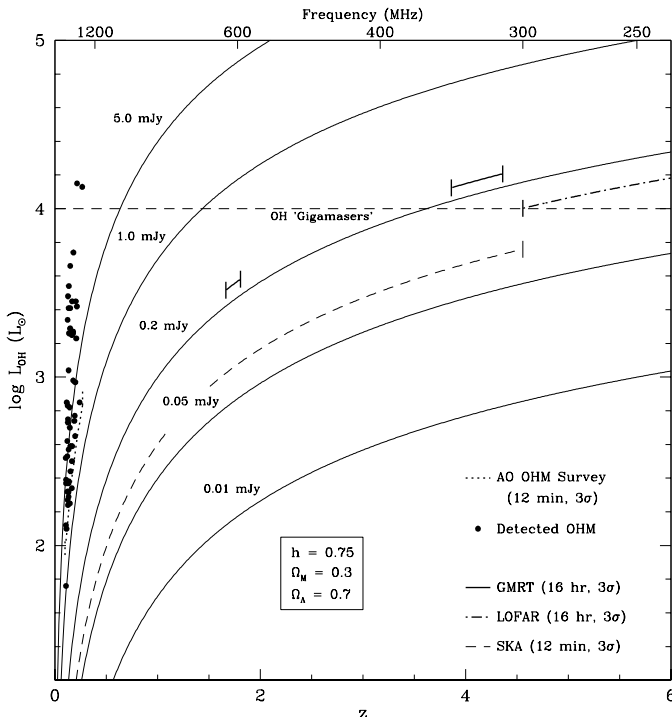


FIG. 4.— Detectability of OH megamasers. Contours show the sensitivity required to detect an OHM with luminosity L_{OH} at redshift z . Included are the results and sensitivity of the Arecibo OHM survey and predictions for the GMRT, the SKA, and LOFAR.

$$= \frac{dV}{d\Omega d\nu} \int \dots \Phi(L_{OH}) d \log L_{OH}. \quad (14)$$

Recall that the OH LF is the number of OHMs with luminosity L_{OH} per Mpc^3 per logarithmic interval in L_{OH} , expressed as

$$\Phi(L_{OH}) = b L_{OH}^a. \quad (15)$$

Hence, the integral in Equation 14 reduces to a simple form

$$\int \dots \Phi(L_{OH}) d \log L_{OH} = \frac{b}{a \ln 10} [L_{OH,max}^a - L_{OH,min}^a(z)]. \quad (16)$$

The volume element per unit solid angle per unit frequency can be translated into the usual panoply of cosmological parameters (Weinberg 1972):

$$\begin{aligned} \frac{dV}{d\Omega d\nu} &= \frac{dz}{d\nu} \frac{dV}{d\Omega dz} \\ &= \frac{dV}{d\Omega dz} \frac{(1+z)^2}{\nu_o} \\ &= \frac{c D_L^2}{H_o \nu_o \sqrt{(1+z)^3 \Omega_M + \Omega_\Lambda}}. \end{aligned} \quad (17)$$

Hence, the final result for the sky density of OHMs in a flat spacetime has the form

$$\begin{aligned} \frac{dN}{d\Omega d\nu} &= \frac{c D_L^2}{H_o \nu_o \sqrt{(1+z)^3 \Omega_M + \Omega_\Lambda}} \frac{b}{a \ln 10} \\ &\times [L_{OH,max}^a - L_{OH,min}^a(z)]. \end{aligned} \quad (18)$$

The minimum detectable L_{OH} depends on the sensitivity of observations and the redshift, as shown in Figure 4. The maximum L_{OH} is assumed to be $10^{4.4} L_\odot$ which is a factor of two larger than the luminosities of the known OH gigamasers. The effects of relaxing this conservative assumption are discussed below. When $L_{OH,min} = L_{OH,max}$ there are no OHMs left to detect.

Finally, we fold in an evolution parameter m which scales the sky density of OHMs as $(1+z)^m$. Assuming $H_o = 75 \text{ km s}^{-1} \text{ Mpc}^{-1}$, $\Omega_M = 0.3$, and $\Omega_\Lambda = 0.7$, and folding in the OH LF parameters a and b from §3, we obtain the sky density of OHMs for any sensitivity level as a function of redshift. The detectable sky density of OHMs versus redshift is plotted in Figure 5 for a 3σ OH line detection at 0.25 mJy. Several evolution scenarios are plotted: $m = 0$ (no evolution), $m = 4$, and $m = 8$. We assume an arbitrary turnover in the evolution factor at $z = 2.2$, after which the number density of OHMs is constant. This turnover in the merger rate corresponds roughly to the turnover in the QSO luminosity function. The point with error bars is a prediction of the sky density of OHMs derived from the space density of submillimeter detections (which are ostensibly ULIRGs) computed by Barger, Cowie, & Richards (2000) assuming that half of the submillimeter galaxies produce detectable OHMs. Bands currently accessible to the GMRT (610 and 327 MHz) in roughly 16 hours of integration are indicated in bold. The proposed Square Kilometer Array might reach the same sensitivity level in a few minutes of integration. If the submillimeter predictions are to be believed, very strong evolution is favored and the GMRT could detect dozens of OHMs per square degree in its 32 MHz bandpass in a reasonable integration time. This is a very exciting prospect and can indicate which models of galaxy evolution are favored, as discussed below.

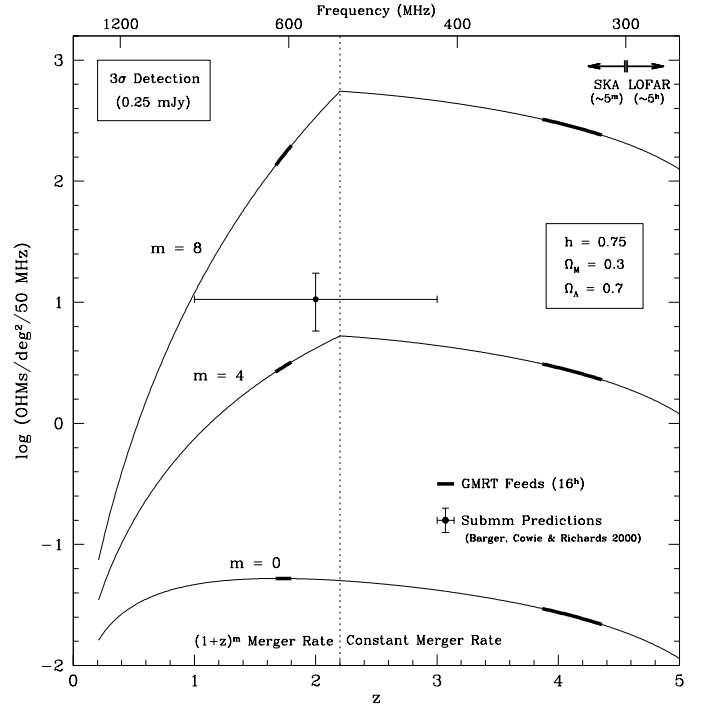


FIG. 5.— Sky density of detectable OH megamasers at 0.25 mJy. The expected detections for several galaxy merger histories are labeled by the rate of increase in the merger rate as $(1+z)^m$. The point with error bars is the prediction for OHM detections based on the space density of submillimeter detections computed by Barger, Cowie, & Richards (2000). The turnover in merger rate from increasing to constant at $z = 2.2$ is indicated by the dotted vertical line. The GMRT (currently accessible bands are indicated in bold) can reach the RMS noise of 0.083 mJy in each 0.12 MHz channel in roughly 16 hours of integration. The proposed SKA might reach the same noise level in a few minutes of integration while LOFAR would require several hours.

Briggs (1998) makes predictions of the sky density of OHMs using the FIR LF of LIRGs of Koranyi & Strauss (1997), a quadratic OH-FIR relation, and an optimistic OHM fraction as a function of $L_{60\mu m}$ derived from Baan (1989) and Baan *et al.* (1992). Briggs predicts roughly 16 OHMs at $z = 2$ per square degree per 50 MHz bandpass for $m = 4.5$ and a sensitivity level of 0.2 mJy. The predictions of OHM detections based on the Arecibo survey OH LF are not as rosy; only about 6 OHMs would be detected for $m = 4.5$ at 0.2 mJy at $z = 2$. The main discrepancy between the two predictions lies in Briggs' use of a quadratic OH-FIR relation and a high OHM fraction in LIRGs compared to the fraction detected in the Arecibo OHM survey.

If the assumptions built into these detection predictions are changed, the results change only slightly below $z \sim 2$. For example, if the OH LF is extended to $L_{OH} = 10^5 L_\odot$, there is no significant effect on the detection rates below $z \sim 3$ because the most luminous OHMs are rare. The detection rates at the highest redshifts will change significantly because only the tail of the OH LF is detected, but predictions beyond $z = 2$ are wild speculations with no supporting data. The choice of cosmology also does not alter the detection rates dramatically. Changing from an $\Omega_\Lambda = 0$ to an $\Omega_\Lambda = 0.7$ universe amounts to roughly a factor of 1.5 increase in OHM detections at $z < 2$. The effect again becomes more significant at higher redshifts.

4.3. The Merging History of Galaxies

A property as basic as the number density of galaxies as a function of redshift is not well known. The number density of galaxies depends of course on the merging history of galaxies, which is an essential ingredient in theories of structure formation and galaxy evolution. There have been a number of studies which attempt to measure the merger rate or merger fraction of galaxies versus redshift, and most of them parameterize the evolution of mergers with a factor $(1+z)^m$. A *Hubble Space Telescope* survey identifying optical mergers and close pairs of galaxies indicates $m = 3.4 \pm 0.6$ from $z = 0$ to $z = 1$ (Le Fèvre *et al.* 2000), whereas the 1 Jy ULIRG survey indicates an exponent of $m = 7.6 \pm 3.2$ (Kim & Sanders 1998) which is similar to the evolution of bright QSOs with redshift as $m \sim 6$ up to $z \sim 2.5$ (Briggs 1998; Hewett *et al.* 1993; Schmidt *et al.* 1995). Semi-analytic models of hierarchical galaxy formation by Kauffmann & Haehnelt (2000) indicate an evolution of the number density of gas-rich mergers from $z = 0$ to $z = 2$ roughly following $m = 4$. The sampling of work on this topic listed here is by no means complete. In general, most studies indicate a strong increase of the merging rate with redshift, but it is likely to be a strong function of the total dark halo mass (for which bolometric luminosity is a proxy) and the mass ratio of the merging pair (Khochfar & Burkert 2001). A luminosity dependence is seen in the evolution of quasars and LIRGs, with the most luminous objects showing the strongest evolution (Schmidt *et al.* 1995; Kim & Sanders 1998).

Although a deep survey for OH megamasers may not be translatable into a merger rate, it does discriminate between various galaxy evolution scenarios. For example, there are two orders of magnitude difference between the OHM detections expected from $m = 8$ versus $m = 4$ at $z \sim 2$. Even a lack of detections in an adequately deep OHM survey would provide new constraints on the evolution of mergers with redshift and would suggest a revision of the conventional interpretation of submm galaxies as high-redshift ULIRGs. If, on the other hand, OHMs were detected in a deep survey, this would not only indicate the evolution of merging but also provide an extinction-free redshift determination for submillimeter galaxies which have proven to be extremely difficult to identify and observe at optical wavelengths or even IR wavelengths (e.g.—Smail *et al.* 2000; Ivison *et al.* 2000).

4.4. The Star Formation History of the Universe

Merging systems traced by OH megamasers are in the throes of extreme starbursts, but much of the star formation is highly obscured by dust. The history of obscured star formation is difficult to determine with current instruments which detect the reprocessed light directly at FIR or submm wavelengths due to poor sensitivity or the difficulty of determining redshifts, respectively. OH megamasers are a promising solution to these limitations because they are luminous, are unattenuated by dust, and provide redshifts. As Townsend *et al.* (2001) point out, OH megamasers may be used to determine the nature and evolution of submm galaxies and to indicate their relevance to the star formation history of the universe. If the connections between OHMs and their hosts, particularly

between L_{OH} and L_{FIR} (or at least the OH LF and the FIR LF), are valid at moderate to high redshifts, then surveys for OHMs can be used as an independent measure of the star formation history across a large span of the age of the universe.

4.5. Constraining The Gravitational Wave Background

One final potential application of OHMs addresses the end result of massive mergers: the formation and coalescence of binary supermassive black holes. Supposing that each galaxy in a merger contains a supermassive black hole, the rapid coalescence of nuclei due to dynamical friction will produce a binary supermassive black hole which will continue to decay until a final coalescence event which will produce (among other things) a burst of gravitational waves. Bursts from supermassive black holes are likely to be the major source of 10^{-5} – 10^0 Hz gravitational waves (Haehnelt 1994) which may someday be detectable by the Laser Interferometer Space Antenna (LISA) or long-duration pulsar timing. The merging rate of galaxies, as well as the masses of the black holes involved, determine the event rate detectable by LISA. The integrated merging history of galaxies determine the noise levels produced in pulsar timing, and would provide a “foreground” to any cosmological background of gravitational waves produced during the inflationary epoch (D. Backer 2001, private communication). Clearly, getting some handle of the event rate of supermassive black hole mergers would provide much needed constraints and thresholds for the difficult work of detecting gravitational waves.

5. SUMMARY

The OH luminosity function constructed from a sample of 50 OH megamasers detected by the Arecibo OH megamaser survey indicates a power-law falloff with increasing OH luminosity

$$\Phi = (9.8^{+31.9}_{-7.5} \times 10^{-6}) L_{OH}^{-0.64 \pm 0.21} \text{ Mpc}^{-3} \text{ dex}^{-1}$$

valid for $2.2 < \log L_{OH} < 3.8$ (expressed in L_{\odot}) and $0.1 < z < 0.23$. The OH LF is used to predict the areal density of detectable OHMs at arbitrary redshift for a manifold of galaxy merger evolution scenarios parameterized by $(1+z)^m$ where $0 < m < 8$. For reasonable choices of m , an “OH Deep Field” obtained with the Giant Metrewave Radio Telescope at 610 MHz ($z = 1.73$) may detect dozens of OHMs per square degree in a reasonable integration time. A lack of detections in a sufficiently deep field would also significantly constrain the evolution of merging and exclude the most extreme evolution scenarios.

The authors are very grateful to Will Saunders for access to the PSCz catalog and to the excellent staff of NAIC for observing assistance and support. We thank the anonymous referee for thoughtful comments and suggestions. This research was supported by Space Science Institute archival grant 8373 and NSF grant AST 00-98526 and made use of the NASA/IPAC Extragalactic Database (NED) which is operated by the Jet Propulsion Laboratory, California Institute of Technology, under contract with the National Aeronautics and Space Administration.

REFERENCES

- Baan, W. A., 1989, ApJ, 338, 804
- Baan, W. A. 1991, ASP Conf. Ser. 16, Atoms, Ions, & Molecules: New Results in Spectral Line Astrophysics (San Francisco: ASP), 45
- Baan, W. A., Haschick, A., & Henkel, C. 1992, AJ, 103, 728
- Barger, A. J., Cowie, L. L., & Richards, E. A. 2000, AJ, 119, 2092
- Briggs, F. H. 1998, A&A, 336, 815
- Condon, J. J., Cotton, W. D., Greisen, E. W., Yin, Q. F., Perley, R. A., Taylor, G. B., & Broderick, J. J. 1998, AJ, 115, 1693
- Dale, D. A., Helou, G., Contursi, A., Silbermann, N. A., & Kolhatkar, S. 2001, ApJ, 549, 215
- Darling, J. & Giovanelli, R. 2000, AJ, 119, 3003 (Paper I)
- Darling, J. & Giovanelli, R. 2001, AJ, 121, 1278 (Paper II)
- Darling, J. & Giovanelli, R. 2002a, AJ, in press (Paper III)
- Fisher, K. B., Huchra, J. P., Strauss, M. A., Davis, M., Yahil, A., & Schlegel, D. 1995, ApJS, 100, 69
- Fullmer, L. & Lonsdale, C. 1989, Cataloged Galaxies and Quasars observed in the IRAS Survey (Version 2; Pasadena: JPL)
- Haehnelt, M. G. 1994, MNRAS, 269, 199
- Hewett, P. C., Foltz, C. B., & Chaffee, F. H. 1993, ApJ, 406, L43
- Iverson, R. J., Smail, I., Barger, A. J., Kneib, J.-P., Blain, A. W., Owen, F. N., Kerr, T. H., & Cowie, L. L. 2000, MNRAS, 315, 209
- Kauffmann, G. & Haehnelt, M. 2000, MNRAS, 311, 576
- Khochfar, S. & Burkert, A. 2001, ApJ, 561, 517
- Kim, D.-C. & Sanders, D. B. 1998, ApJS, 119, 41
- Koranyi, D. M. & Strauss, M. A. 1997, ApJ, 477, 36
- Lawrence, A., et al. 1999, MNRAS, 308, 897
- Le Fèvre, O., et al. 2000, MNRAS, 311, 565
- Lineweaver, C. H., Tenorio, L., Smoot, G. F., Keegstra, P., Banday, A. J., & Lubin, P. 1996, ApJ, 470, 38
- Lu, N. Y. & Freudling, W. 1995, ApJ, 449, 527
- Page, M. J. & Carrera, F. J. 2000, MNRAS, 311, 433
- Saunders, W., et al. 2000, MNRAS, 317, 55
- Schmidt, M. 1968, ApJ, 151, 393
- Schmidt, M., Schneider, D. P., & Gunn, J. E. 1995, AJ, 110, 68
- Smail, I., Iverson, R. J., Owen, F. N., Blain, A. W., & Kneib, J.-P. 2000, ApJ, 528, 612
- Staveley-Smith, L., Norris, R. P., Chapman, J. M., Allen, D. A., Whiteoak, J. B., & Roy, A. L. 1992, MNRAS, 258, 725
- Strauss, M. A., Huchra, J. P., Davis, M., Yahil, A., Fisher, K. B., & Tonry, J. 1992, ApJS, 83, 29
- Townsend, R. H. D., Iverson, R. J., Smail, I., Blain, A. W., & Frayer, D. T. 2001, MNRAS, in press (astro-ph/0106112)
- Weinberg, S. 1972, *Gravitation and Cosmology*, John Wiley & Sons, New York
- Yun, M. S., Reddy, N. A., & Condon, J. J. 2001, ApJ, 554, 803